JTTEE5 19:521–530
DOI: 10.1007/s11666-009-9464-5
1059-9630/$19.00 © ASM International

Effects of HVOF Process Parameters on the Properties of Ni-Cr Coatings

J. Saaedi, T.W. Coyle, H. Arabi, S. Mirdamadi, and J. Mostaghimi

(Submitted December 13, 2008; in revised form November 4, 2009)

This research examined the influence of processing parameters on the structure of a Ni-50Cr coating applied by high-velocity oxy-fuel spraying onto stainless steel specimens. This type of coating is normally used as protection against heat and corrosion encountered in power plant and marine boilers, and oil refinery heaters. A statistical design of experiments identified fuel and oxygen flow rates and spraying distance as the most influential parameters controlling the in-flight characteristics of the powder particles prior to impact. The effects of these parameters on the porosity level, oxide content, and microhardness of the coatings were then investigated in more detail. These results indicated that the oxide content and hardness of the coatings were dependent on the gas combustion ratio but not on spraying distance. The porosity level and amount of unmelted particles were reduced at the longest spraying distance.

Keywords fuel-to-oxygen ratio, HVOF, Ni-Cr coatings, oxide content, spraying distance

1. Introduction

Nickel-chromium alloys are used as coatings to deal with oxidation and corrosive environments at high temperatures. Nickel alloys containing more than 30% chromium are extremely difficult to fabricate by conventional hot working processes because of the development of a brittle alpha chromium phase (Ref 1). Ni-50Cr has been a standard casting alloy for heat-resistant and elevated-temperature corrosion applications up to 1090 °C since 1972 (Ref 2). This alloy is a well-established material for resisting oil ash corrosion in power plants, oil refinery heaters, and marine boilers involving temperatures less than about 900 °C (Ref 3). Furthermore, positive experience has been reported on the use of this alloy as a metal dusting resistant coating (Ref 4). A high-velocity oxy-fuel (HVOF) sprayed 50Ni-50Cr coating was reported to yield good protection up to 750 °C in ultra-supercritical (USC) boiler components (Ref 5).

Thermal spray coatings are often applied to improve corrosion and wear resistance. The coatings used at higher temperatures must be dense enough that any residual voids can be filled by formation of protective oxides and be thick enough to postpone the diffusion of corrosive species to the substrate material until protective oxides form within the coating (Ref 6).

For those materials that are sensitive to changes in composition due to evaporation or oxidation, HVOF spray is an attractive coating method due to the process conditions, which combine a relatively low-flame temperature with a low-exposure time (short dwell time) in the flame (Ref 7). It uses high-pressure combustion of a fuel (propylene, acetylene, propane, or hydrogen gases) to produce a gas temperature greater than 3029 K and to generate a supersonic or hypersonic gas velocity of approximately 2000 m/s, more than five times speed of sound (Ref 8).

HVOF coatings are homogeneous and dense compared to the other types of thermal-sprayed coatings, nevertheless some residual oxides and porosity remain at splat boundaries. These inhomogeneities decrease the corrosion resistance of the coatings. In addition, gas-phase corrosion may cause severe corrosion of HVOF-coated components when the coatings are permeable to the corrosive gases (Ref 9).

Designing deposits with suitable properties requires a general understanding of the coating processes, i.e., spraying techniques and their parameters, knowledge of the resulting microstructure, and also of the relationships between microstructure and the properties of the deposits. Optimization of a coating for a particular application requires finding a coating with the proper combination of properties. This usually means that the microstructure of the deposits needs to be optimized (Ref 10). The microstructure and physical properties of the coatings are determined by the physical and chemical properties of the particles impinging on the substrates, which in turn are dependent on a large number of parameters such as gun design, the fuel/oxygen ratio, the position of the substrate relative to the gun, the particle size and shape, injection

J. Saaedi, Centre for Advanced Coating Technologies, Department of Materials Science and Engineering, University of Toronto, 184 College Street, Toronto, ON M5S 3E4, Canada and Department of Materials and Metallurgical Engineering, Iran University of Science and Technology, Tehran, Iran; **T.W. Coyle** and **J. Mostaghimi**, Centre for Advanced Coating Technologies, Department of Materials Science and Engineering, University of Toronto, 184 College Street, Toronto, ON M5S 3E4, Canada; and **H. Arabi** and **S. Mirdamadi**, Department of Materials and Metallurgical Engineering, Iran University of Science and Technology, Tehran, Iran. Contact e-mail: jahan.saaedi@utoronto.ca.

method, and so on. Hence, to successfully apply the HVOF technique, it is necessary to optimize these parameters (Ref 8). In the HVOF process, the particles may melt completely or partially. This depends on the flame temperature, the residence time, and material's melting point and affects the properties of the coating (Ref 11). The flame temperature and residence time depend on adjustable process parameters. A good understanding of the relationship of these variables and their effect on the coating properties must be obtained in order to apply thermal spray coating to ''prime reliant'' applications (Ref 7).

In this study the effects of five important spraying process parameters, including the fuel/oxygen ratio and spraying distance (SD), on the microstructural properties and hardness of Ni-50Cr coatings deposited by HVOF spraying were investigated. To date, only a small number of studies have been reported in the open literature focused on the relationships between HVOF process parameters and properties of Ni-50Cr and similar alloys. Therefore, the technical goal of this work was to define the effects of critical process parameters on coating microstructures which could be used as guidance for optimization of coating performance of this alloy under corrosive environments.

2. Experimental Details

2.1 Materials and HVOF Spraying

A commercial gas atomized Ni-50Cr powder (Sulzer Metco Inc., Fort Saskatchewan, Alberta) was used for the study. The typical composition and particle size according to the supplier's data are shown in Table 1. A Sulzer Metco DJ 2700 Diamond Jet Gun with propylene as fuel gas was employed for spraying. Powder was fed to the gun using a nitrogen carrier gas with flow rate of 9 SLM.

A Taguchi-style, orthogonal L8 experimental design was employed in a preliminary screening study to evaluate the effect of five processing parameters (oxygen flow, fuel flow, air flow, spraying distance, and feed rate) on the in-flight particle temperature and velocity. These two sprayed particle characteristics, along with substrate temperature and surface finish, are the main factors affecting the splat morphology and resulting coating properties (Ref 12-14). A DPV-2000 (Tecnar Automation Ltèe, St-Bruno, Canada) diagnostic system was utilized to determine particle temperature and velocity at the specified distance from the gun exit. The data from all runs were included in the analysis of variance (ANOVA) evaluations.

Eight combinations of five process parameters, each with two levels, were employed for spraying of the Ni-50Cr powder. The design matrix is described in Table 2, where a plus sign denotes the high level and a minus sign the low level of the respective parameters. The high and low levels of each parameter are given in Table 3. The levels of fuel flow and oxygen flow were selected so that the corresponding fuel/oxygen ratios ranged from about 10% below to about 30% above the stoichiometric ratio of 0.22 for propylene-oxygen combustion. The fuel/oxygen ratio does not include consideration of the oxygen contained in the air introduced around the periphery of the chamber.

Evaluation of the results of the Taguchi DOE identified the process parameters which had the most significant effects on the in-flight particle temperature and velocity. Fuel flow, oxygen flow, and spraying distance were found to be the critical process parameters; therefore, subsequent experimental trials focused on the effects of these parameters.

The desired particle characteristics of low temperature and high velocity were favored by the high fuel flow setting, so in the second set of experiments the fuel flow was held constant at this upper level (85 SLM) while oxygen flow was varied. The fuel flow and oxygen flow were taken into consideration in one parameter as the fuel/oxygen ratio to emphasize the combustion condition in the gun

Table 1 The manufacturer's specifications of the powder used

	Property						
	Composition, wt.%						
Powder	C	Cr	Fe	Mn	Si	Ni	Nominal size
Ni-50Cr	0.03	49.6	0.1	0.1	0.3	Bal.	−44 μm

Table 2 Taguchi-style, orthogonal L8 design matrix used in this research

Experiment no.	Oxygen flow	Fuel flow	Air flow	Spraying distance	Feed rate
1	−	−	−	−	−
2	−	−	−	+	+
3	−	+	+	−	−
4	−	+	+	+	+
5	+	−	+	−	+
6	+	−	+	+	−
7	+	+	−	−	+
8	+	+	−	+	−

Table 3 The process parameters investigated

Parameter	Oxygen flow, SLM	Fuel flow, SLM	Air flow, SLM	Spraying distance, mm	Feed rate, g/min
Minimum value	300	60	355	200	23
Maximum value	350	85	405	300	34

SLM, Standard liters per minute

Table 4 Process parameters for the second set of experiments

Trial	Parameter				
	Fuel flow, SLM	Oxygen flow, SLM	Fuel/ oxygen ratio	Spraying distance, mm	Substrate surface speed, m/min
1	85	300	0.28	200	17.2
2	85	300	0.28	230	14.3
3	85	300	0.28	265	10.7
4	85	283	0.3	150	22.0
5	85	283	0.3	175	19.5
6	85	283	0.3	200	17.2
7	85	283	0.3	230	14.3
8	85	243	0.35	150	22.0
9	85	243	0.35	175	19.5
10	85	243	0.35	200	17.2
11	85	243	0.35	230	14.3
12	85	170	0.5	150	22.0
13	85	170	0.5	230	14.3
14	85	170	0.5	265	10.7
15	85	170	0.5	300	6.4
16	85	142	0.6	150	22.0
17	85	142	0.6	230	14.3
18	85	142	0.6	265	10.7
19	85	142	0.6	300	6.4

relative to the ideal stoichiometric condition. Fuel-rich combustion conditions compared to the stoichiometric fuel/oxygen ratio of 0.22 were chosen: 0.28, 0.3, 0.35, 0.5, and 0.6. Spraying distances of 150, 175, 200, 230, 265, and 300 mm were selected. The air flow and powder feed rate, which were found to be relatively insignificant parameters, were held constant at 355 SLM and 23 g/min for all depositions. The thickness of the coatings ranged from 180 to 320 μm depending on the spray parameters used for each specimen. The process parameters used for the second set of experiments and corresponding fuel/oxygen ratios are shown in Table 4.

For each spraying condition, a number of stainless steel substrates were mounted on a turntable placed in front of the gun. The substrates were grit blasted and cleaned by acetone before coating. Substrates were mounted at various positions along the radius of the turntable so that depositions could be made simultaneously at four different spraying distances. The rotation rate of the turntable during spraying was 100 rpm. The gun, mounted on a programmable robotic system was aligned perpendicular to the turntable axis of rotation and moved up and down the axis at a speed of 12.7 mm/s. In this way, flat substrates typically 50 mm by 70 mm by 3 mm thick were coated. The DPV2000 was employed to measure in-flight particle velocity and temperature for some, but not all, deposition conditions. To avoid over heating, the substrates were cooled by compressed air directed onto the substrate through a pair of nozzles during spraying. The temperature of the substrates mounted on the rotating turntable could not be measured during deposition with the equipment available; however, no red glow was visible from the substrates during deposition indicating the temperature did not exceed ~500 °C. The substrate temperature was sufficient to allow oxidation of the stainless steel substrate to occur during deposition since changes were observed in the interference color of the back surfaces of the substrates after deposition.

2.2 Characterization

The powder particle size distribution was determined using a Malvern Mastersizer (Malvern Instruments Ltd., Malvern, UK) particle size analyzer. Powder particle morphologies were studied in a scanning electron microscope (SEM) by sprinkling a small quantity of the powder onto an adhesive stub and then images were obtained using the secondary electron signal. The SEM used in this work was a JEOL JSM-840. Cross sections were cut from coated samples, mounted in resin, and then prepared by standard metallographic procedures for examination by optical microscopy (OM).

Image analysis software (Clemex Technologies Inc., Longueuil, Canada) was utilized to quantify the area fraction of porosity and unmelted particles in the coatings. Images for image analysis were obtained from as-polished surfaces using differential interference-contrast in the optical microscope. Under these imaging conditions, the oxides in the coating had a gray contrast which could be distinguished from the black contrast of the pores (Ref 15). To determine the amount of porosity and unmelted particles in the coatings, 10-12 images at a magnification of 600× were taken at different locations on each coating sample and the average of the results reported. Circular and semicircular cross-sectional particle shapes (spherical and dome shaped in three-dimensional space) were considered as unmelted particles. Image processing tools were utilized to differentiate unmelted particles from the surrounding coating and then the area fraction of unmelted particles was determined by thresholding them with the image analysis software.

The oxygen content of the coatings and feedstock powder was determined by the inert gas fusion technique, using a Leco Oxygen/Nitrogen Analyzer, Model TC-136 (Leco Corporation, St. Joseph, MI). Three to five measurements were conducted and averaged for every specimen.

Vickers hardness measurements were performed to assess the coating hardness on the polished cross sections using a Leitz Wetzlar microhardness tester with a load of either 100 or 500 g. The load of 100 g was used for measuring the microhardness of unmelted particles. To measure coating microhardness which would be as close as possible to overall hardness of coating, a load of 500 g was employed. Each microhardness value was obtained from an average value of 20 tests.

3. Results

3.1 Ni-50 Cr Powder

The secondary electron images of the powder mixture revealed a broad particle size distribution (Fig. 1a). The majority of the particles in the powder mixture have a

near-spherical morphology, typical of powder produced by inert gas atomization. The particle size ranged from 10 to 55 μm, with a median particle size of 35 μm. Moreover, about 25 vol.% of the powder particles was smaller than 20 μm (Fig. 1b). The oxygen content of the powder was found to be 0.16 wt.%.

3.2 ANOVA Evaluation of Particle Temperature and Velocity Measurements

Table 5 illustrates the results of particle temperature and velocity measurements for the experiments conducted according to the DOE matrix array in Table 2.

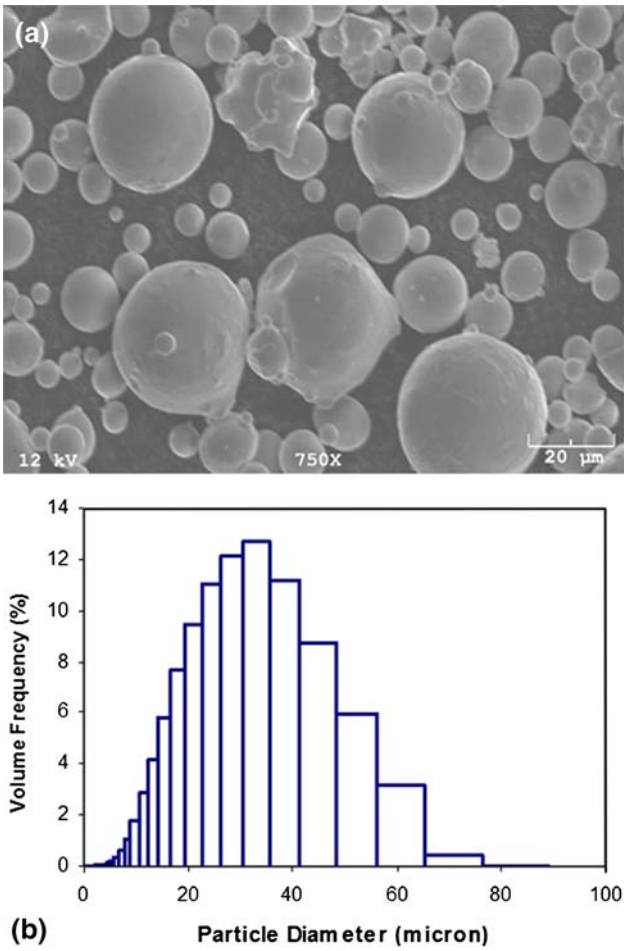

Fig. 1 SEM micrograph of the Ni-50Cr powder (a), and particle size distribution (b)

The ANOVA analysis of the HVOF thermal spray process statistically delineated the impact of each factor on the measured particle characteristics across all combinations of other factors. The mean of the trial results are used to calculate the average effect of each factor at each of its levels. From the ANOVA calculations, the rho percent contribution (ρ, %) of each variable was determined for the measured particle temperature and velocity, thereby giving us an insight into the relationship between the variables and particle properties. The ρ value indicates the influence of the process parameter on the measured response, with a larger number indicating stronger influence. The ρ% denotes the percentage of the total variance of each individual factor and is defined as the pure sum of squares of factors divided by the total sum of squares. For any individual factor, the pure sum of squares is $S'_m = S_m - D_m \times V_e$, where S'_m, S_m, D_m, and V_e denotes the corresponding pure sum of squares, sum of squares, degree of freedom, and error variance, respectively (Ref 16). Table 6 illustrates the results of the Taguchi analysis.

The spraying distance and fuel flow have the most significant effects on the in-flight particle temperature, although the error factor (due to measurement error and uncontrolled factors) is significant. The in-flight particle velocity was most influenced by fuel flow (i.e., 65.5 ρ%). Oxygen flow and spraying distance were also significant. The effects of feed rate, air flow and the error factor are <5%. Fuel flow, oxygen flow, and spraying distance were therefore identified as the parameters which have the most influence on in-flight particle characteristics, and were selected as the critical process parameters for further coating process development.

3.3 Ni-50Cr Coatings

3.3.1 Microstructure of the As-Deposited Coatings. A detailed analysis of the as-sprayed structure of coatings deposited with this powder has been reported elsewhere (Ref 15); the main characteristics are reviewed in the following. For the coatings deposited with an *F*/*O* ratio of 0.35 or less, a majority of the powder particles were completely melted and deformed extensively on impact to form elongated lamellae (Fig. 2a and b). Few unmelted particles were observed (generally <3 vol.%). The coatings were dense with porosity levels <1 vol.%. The pore size was in the range of 0.8-4 μm. The amount of oxide (gray phases) in the coatings was relatively high, and oxide phases are clearly evident adjacent to the particles which were completely melted.

For the coatings deposited with *F*/*O* ratios of 0.5 and 0.6, the oxide content decreased significantly but the

Table 5 Particle temperature and velocity measurements obtained by the on-line diagnostic system (DPV) (a)

Experiment no.:	1	2	3	4	5	6	7	8
Particle temperature, °C	2208 ± 162	2229 ± 141	2120 ± 182	2215 ± 142	2188 ± 165	2233 ± 136	2070 ± 203	2221 ± 139
Particle velocity, m/s	536 ± 103	517 ± 64	635 ± 112	601 ± 97	599 ± 84	553 ± 72	678 ± 107	618 ± 85

(a) Mean ± standard deviation

Table 6 ANOVA analysis of the Taguchi L8 data

Desired attribute		Oxygen flow	Fuel flow	Air flow	Spraying distance	Feed rate	Other/error
Low temperature	Sums of squares	450	6728	98	12168	800	4178
	Variance	450	6728	98	12168	800	2089
	F-ratio	0.215	3.22	0.046	5.824	0.382	
	Pure sum	0	4639	0	10079	0	
	ρ-Percent	**0**	**18.995**	**0**	**41.27**	**0**	**39.735**
High velocity	Sums of squares	3160.125	13366.125	190.125	3160.125	351.125	105.250
	Variance	3160.125	13366.125	190.125	3160.125	351.125	52.625
	F-ratio	60.049	253.988	3.612	60.049	6.672	
	Pure sum	3107.5	13313.5	37.5	3107.5	298.5	
	ρ-Percent	**15.283**	**65.477**	**0.676**	**15.283**	**1.468**	**1.813**

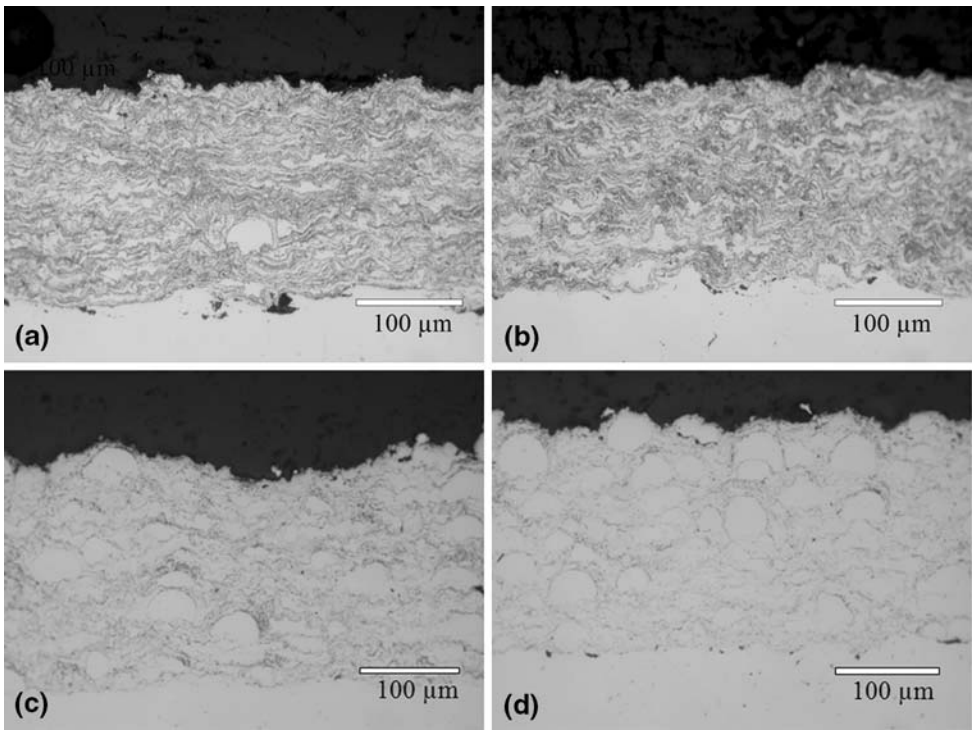

Fig. 2 Optical micrographs obtained using differential interference-contrast of coatings deposited at a spraying distance of 230 mm with a fuel flow of 85 SLM and *F*/*O* ratios of: (a) 0.3, (b) 0.35, (c) 0.5, and (d) 0.6

coatings contained a fairly large amount of unmelted particles (Fig. 2c and d). The porosity was higher than in the lower *F*/*O* ratio coatings and the pore size slightly larger, ranging from 0.8 to 6 µm. Oxide phases were present at intersplat boundaries and at the periphery of the particles that did not flatten on impact. The striking major differences between the two coating microstructures are the amount of oxide and unmelted particles.

Microstructural variations in terms of porosity, oxide, and unmelted particle amounts at different spraying distances were not evident by comparison of OM images although the amount of unmelted particles appeared to be reduced at the longest spraying distance (Fig. 3).

3.3.2 Oxygen Content. No correlation between the spraying distance and the oxygen content was seen which indicates that spraying distance does not play a major role in the oxygen content of the coatings. The formation of oxides on particles in-flight depends on the flame temperature and contact time with oxygen (Ref 17). With a longer spray distance, the sprayed powder has more time to react with the air entrained in the flame, which would result in an increase in oxide content with spray distance. On the other hand, heating of the substrate and previously deposited material by the torch during spraying would increase the oxidation of the recently deposited coating at short spraying distances (Ref 18).

The fuel-to-oxygen ratio has a major effect on the oxygen content of the coatings as can be clearly seen in Fig. 4. The oxygen content of the feedstock powder (0.16 wt.%) was much lower than that of any of the

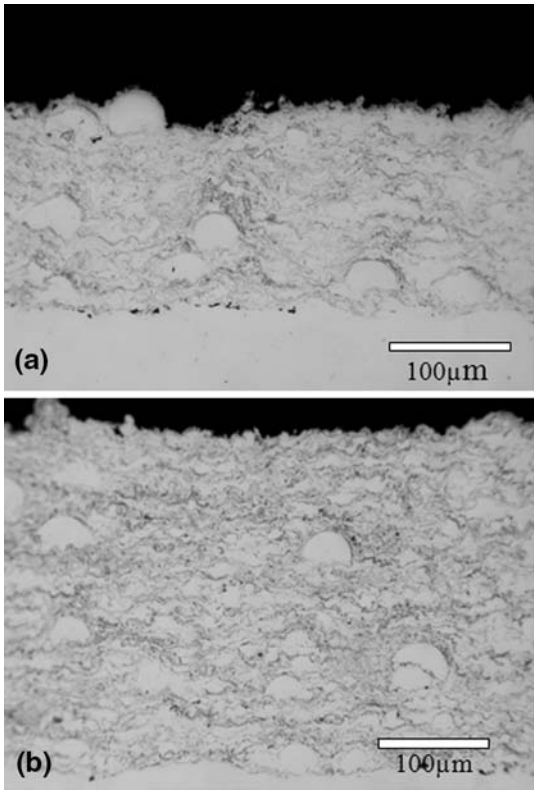

Fig. 3 Optical micrographs obtained from the coatings which deposited by shortest and longest spraying distances with the *F*/*O* ratio of 0.5: (a) 150 and (b) 300 mm

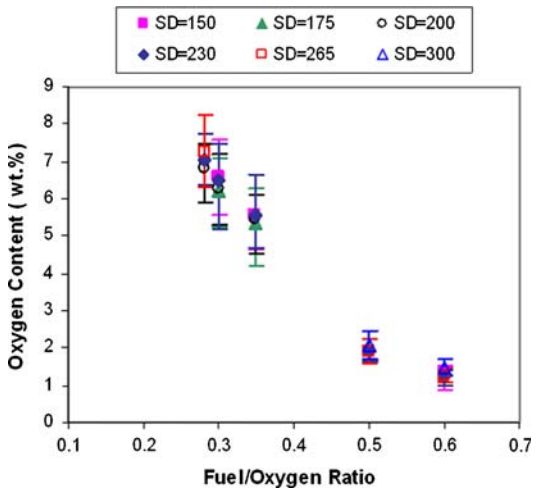

Fig. 4 Oxygen content as a function of fuel/oxygen ratio in the coatings sprayed using different spraying distances. Error bars indicate the range of values obtained in three to five measurements for each sample

coatings, indicating that the oxygen was absorbed during spraying. The results show the importance of controlling the combustion conditions in the spray gun. Spraying the powder with a *F*/*O* ratio of 0.28 led to coatings with an oxygen content of around 7 wt.%. If it is assumed that the

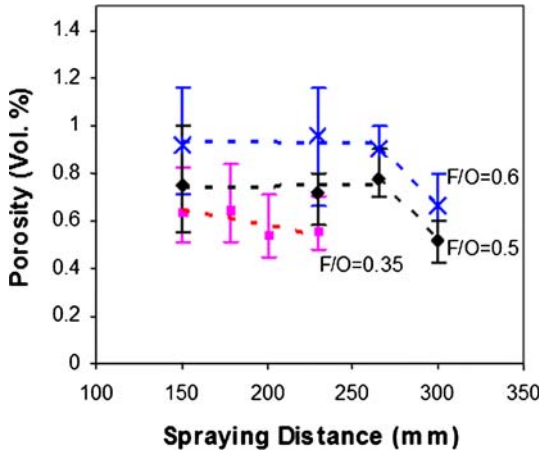

Fig. 5 Porosity level vs. spray distance. Error bars indicate the range of measured values for each sample

total measured oxygen content exists in the form of Cr_2O_3 or $NiCr_2O_4$, the average oxide contents of these coatings would be between 22.1 and 24.7 wt.%. However, some oxygen may exist as gas trapped within the splat boundaries or other pores. By increasing the *F*/*O* ratio, the oxygen level within the coatings decreased to about 1 wt.% for a *F*/*O* ratio of 0.6 which would correspond to 3.2-3.5 wt.% of Cr_2O_3 or $NiCr_2O_4$.

3.3.3 Porosity, Hardness, and Unmelted Particles. The variation of porosity level in the coating as a function of *F*/*O* ratio and spraying distance is shown in Fig. 5. By increasing the *F*/*O* ratio, the average porosity increased from 0.4 to 1 vol.%. For the coatings with an *F*/*O* ratio of 0.35, the porosity was low and not sensitive to the spraying distance. For *F*/*O* ratios of 0.5 and 0.6, the porosity levels were constant for spraying distances up to 250 mm, but decreased at 300 mm.

Figures 6 and 7 show the influences of spraying distance and *F*/*O* ratio on the amount of unmelted particles and hardness of as-sprayed Ni-50Cr coatings. The spraying distance does not play a significant role on the coating hardness, while the amount of unmelted particles is constant up to 250 mm, then decreases at the longest spraying distance. This latter effect is more obvious for highest fuel-to-oxygen ratios.

4. Discussion

The theoretical flame temperatures and excess (unreacted) oxygen in the flame as a function of the amount of oxygen added to the fuel for propylene combustion, as calculated by Hewitt (Ref 19), are shown in Fig. 8. As noted by Hewitt (Ref 19), these temperatures are theoretical and assume equilibrium and adiabatic conditions; considering radiation losses and other factors the actual temperatures would be lower. The excess oxygen in the flame has been scaled as a percentage of the stoichiometric amount of oxygen. The stoichiometric reaction for

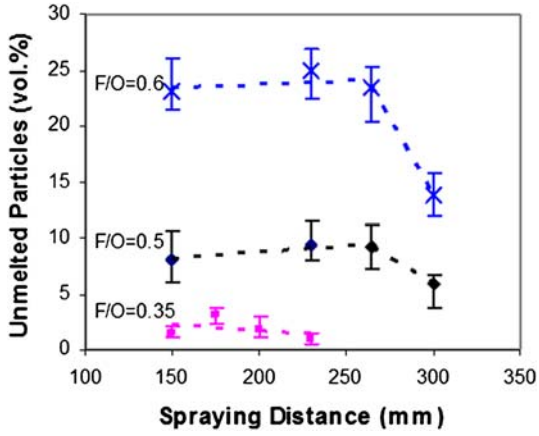

Fig. 6 Unmelted particles amounts within the coating vs. spraying distance. Error bars indicate the range of measured values for each sample

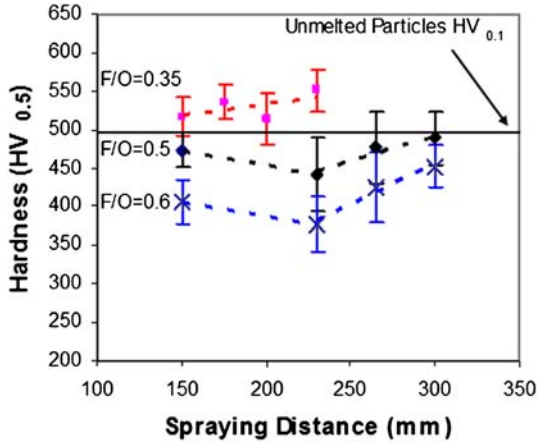

Fig. 7 Coating hardness vs. spraying distance. Error bars represent ±standard deviation about the average value based on at least 20 measurements for each coating

propylene is $C_3H_6 + 4.5O_2 \rightarrow 3CO_2 + 3H_2O$ giving a stoichiometric C_3H_6:O_2 ratio of 0.22. The fuel/oxygen ratios used in this study, which do not include consideration of oxygen from the air introduced into the gun or entrained from the ambient air, are shown as dashed vertical lines in Fig. 8. It is clear that for the two extreme fuel-rich ratios employed in this study, i.e., 0.5 and 0.6, the chemical nature of the flame was reducing and there should not have been excess oxygen available in the flame to drive oxidation of the metallic powder particles. The corresponding flame temperatures for these ratios can be estimated from Fig. 8 as 2460 and 2075 °C, respectively. For the *F*/*O* ratios of 0.28 and 0.3, the flame temperature (2885 °C) would have been near the maximum, with approximately 8.6 and 6.4% excess oxygen available in the flame.

The average in-flight particle temperatures measured for the range of *F*/*O* ratios and spraying distances investigated in this study are shown in Fig. 9(a), plotted in the

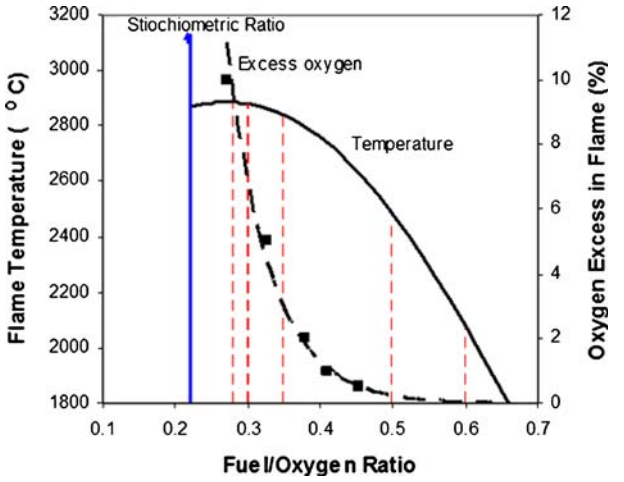

Fig. 8 Calculated flame temperature and excess oxygen in the flame is plotted vs. fuel/oxygen ratio for the combustion of propylene (drawn from data of Ref 19). The vertical lines show the fuel/oxygen ratios used in this study

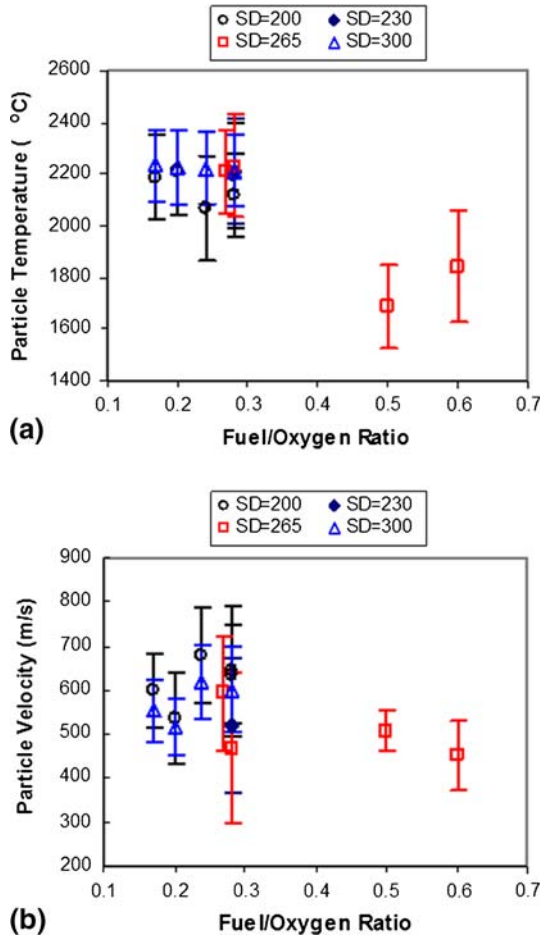

Fig. 9 The average in-flight particle characteristics measured at several spraying distances: (a) particle temperature vs. *F*/*O* and (b) particle velocity vs. *F*/*O*

same format as Fig. 8. The error bars represent ±1 standard deviation about the average. Particle temperature is expected to increase with residence time in the flame and therefore with spraying distance until, at large spraying distances, the flame temperature would begin to decrease (Ref 20, 21). However, the particle temperature measurements made during this study indicate that spraying distance has no significant effect on the average particle temperature, given the size of the error bars. This may be due to heating of the particle surface as a result of exothermic oxidation reactions (Ref 18) and/or changes in particle spectral emissivity as a result oxidation in-flight compensating for the expected particle cooling.

The measured average particle temperature was 2100-2200 °C for *F*/*O* ratios below 0.3, independent of *F*/*O* ratio. This is consistent with the calculations of the effect of *F*/*O* ratio on flame temperature for *F*/*O* ratios approaching the stoichiometric value (see Fig. 8). Under these conditions, almost all of the particles would be melted. The flame temperature is predicted to drop rapidly when the *F*/*O* ratio increases above 0.35. The measured average particle temperatures at these *F*/*O* ratios were 1700-1850 °C, again consistent with Fig. 8.

The average in-flight particle velocities measured for the range of *F*/*O* ratios and spraying distances investigated are shown in Fig. 9(b). A slight decrease in average velocity with increasing *F*/*O* ratio is suggested, although the scatter is relatively large. This is likely related to the decrease in oxygen flow (and therefore total gas flow) for these conditions. No dependence of particle velocity on spraying distance could be discerned within the precision of the velocity measurements, although the initial DOE results indicated that this factor was significant.

The higher oxide content in the coatings deposited at *F*/*O* ratios <0.35 are clearly correlated with the higher in-flight particle temperatures observed under these conditions and the increase in unburned oxygen in the flame indicated in Fig. 8. The reduction in the number of unmelted particles, the decrease in porosity, and the increase in hardness observed for the lower *F*/*O* ratios independent of spraying distance can also be attributed to the higher average particle temperatures under these conditions.

Oxidation in thermal spraying can occur in three steps (Ref 22, 23): (a) in the ''core'' region of the flame, where oxygen is made available by the combustion products; (b) by interaction with ambient atmosphere that is entrained in the flame while the particles are in-flight; and (c) after impact, during solidification and cooling of the particles recently deposited on the substrate. Dobler et al. (Ref 24) have stated that the contribution of these different oxidation steps to the oxygen content of a coating depends not only upon the spray parameters, but also on the spray metal feedstock. Hackett et al. (Ref 22) concluded that primary oxidation of sprayed aluminum coatings occurs on the substrate due to the hot HVOF jet (Step c). Recent work by Korpiola (Ref 25) has shown that oxidation is also possible in the nozzle and about 70% of the oxidation of the HVOF NiCr80/20 coatings was related to oxidation of particles in the nozzle. Our results indicated that the oxygen content of Ni-50Cr coatings could be decreased by about 85% when the *F*/*O* ratio is changed from 0.28 to 0.6. This shows the importance of combustion chemistry in controlling oxidation. However, the oxygen content did not vary significantly with spraying distance within the range of spraying distance examined in this study. This indicates that the residence time of the particles in the flame during flight was not the sole determinant of the extent of oxidation.

If oxidation occurred only during flight (Step a), the oxygen content of the coating would increase with increased spraying distance (increased residence time). If oxidation occurred primarily during solidification and cooling immediately after deposition on the substrate (Step c), the oxygen content of the coating would increase with decreased spraying distance since the coating would be exposed to higher temperature gases from the flame. It appears that these two trends counteract each other in this study, resulting in an oxygen content independent of spraying distance.

According to Fig. 8, no unburned oxygen would be available in the core of the flame at *F*/*O* ratios of 0.5 and above. Air which turbulently mixes into the flame could contribute to oxidation in Steps (b) and (c). The oxygen content of the coatings deposited using *F*/*O* ratios of 0.5 and 0.6 (1-2 wt.% O) may then be attributed to oxidation of the particles in the latter stages of flight (Step b) and during solidification and cooling immediately after deposition on the substrate (Step c) due to air entrained in the flame.

The microhardness of a coating depends on a combination of the volume fraction of unmelted particles (V_u), porosity, residual stresses, and oxide inclusions. The lower hardness and high volume fraction of unmelted particles in the coatings deposited with the higher *F*/*O* ratios (Fig. 6 and 7) can be related to the lower flame temperature (Fig. 8). The microhardness of individual unmelted particles was measured using a load of 100 g and found to be 498 HV0.1. Therefore, the presence of unmelted particles does not explain the lower microhardness of coatings deposited at *F*/*O* ratios of 0.6 and 0.5. Microhardness is highly sensitive to the level of porosity (Ref 26, 27), and a part of the total porosity of the coating can be attributed to the pores associated with the unmelted particles (Ref 26). Therefore, the low microhardness in coatings with a high volume fraction of unmelted particles was due to the presence of porosity associated with the unmelted particles. The higher microhardness of the coatings deposited with an *F*/*O* ratio of 0.35 relative to that of unmelted particles may be attributed to the high oxide contents of these coatings (Fig. 7).

The coatings deposited at a spraying distance of 300 mm were found to contain fewer unmelted particles and lower porosity than the trends would have suggested (Fig. 5 and 6). A corresponding increase in hardness is suggested, although the scatter is large. This may be due to peening of the coating by unmelted particles that were, at this distance, too cold to be incorporated in the coating. The translation speed of the substrate relative to the torch was significantly slower at this spraying distance (6.4 mm/min,

see Table 4) than for the shorter spraying distances; however, the influence of this parameter could not be assessed in detail.

5. Conclusions

The following conclusions can be drawn from this research:

- Fuel flow, spraying distance, and oxygen flow were the most important HVOF process parameters affecting the in-flight particle temperature and velocity. Feed rate and air flow were found to have insignificant effects over the range examined.
- The spraying distance did not play a significant role on the oxygen content of the coatings, but an obvious correlation between fuel-to-oxygen ratio and oxygen content was observed.
- Using a fuel-to-oxygen ratio of 0.35 (1.6 times the stoichiometric amount of oxygen) or less for spraying Ni-50Cr powder resulted in high in-flight particle temperatures and dense coatings with a relatively high oxide content. The microhardness of these coatings was higher than that of the feedstock powder due to the presence of ~7 wt.% of oxygen in the coatings.
- A much higher *F*/*O* ratio (more than 0.5) reduced the in-flight particle temperature by 200-400 °C and the amount of oxygen available in the flame. This was beneficial for minimizing the oxide content, but under these conditions the coatings contained a fairly large amount of retained unmelted particles. The minimum oxide content was found to be within the range of 3.2-3.5 wt.% when using an *F*/*O* ratio of 0.6.
- Oxidation in the coatings deposited with *F*/*O* ratios of 0.35 and less occurred in all stages of the process, i.e., in the combustion chamber and nozzle, in the plume, and on substrate, but in the case of the higher *F*/*O* ratios, 0.5 and 0.6, it occurred primarily after impact of the particles on the substrate.
- The average porosity increased from 0.4 to 1 vol.% as the fuel-to-oxygen ratio increased from 0.28 to 0.6. At a given *F*/*O* ratio, the particle temperature, particle velocity, oxide content, porosity, and the amount of unmelted particles did not vary significantly with spraying distance, except at the spraying distance (300 mm), where the porosity and number of unmelted particles were reduced.

Acknowledgments

Thanks are expressed to Dr. Larry Pershin and Tiegang Li for help with deposition of the coatings. Partial support for J. Saaedi during the course of this work was provided by the Centre for Advanced Coating Technologies (Prof. Javad Mostaghimi, Director).

References

1. D.A. Shifler and L.K. Kohler, Hot Corrosion Resistance and Thermal Stability of High Chromium-Nickel Alloys, *Presented at and Published in Proceedings of the NACE International Annual Conference CORROSION/2000*, Paper no. 242, NACE, Houston, Texas, 2000
2. "Standard Specification for Casting, Chromium-Nickel Alloys, A560," *Annual Book of ASTM Standards*, ASTM, 2000
3. J.R. Davis, Ed., *Heat-Resistant Materials: ASM Specialty Handbook*, ASM, Materials Park, OH, 1997, p 383-384
4. H.L. Holland, Practical Experience with Countering Metal Dusting in a Methane Reforming Unit, *Presented at and Published in Proceedings of the NACE International Annual Conference CORROSION/2001*, Paper No. 1385, NACE, Houston, TX, 2001
5. T. Sundararajan, S. Kuroda, and F. Abe, Effect of Thermal Spray on the Microstructure and Adhesive Strength of High-Velocity Oxy-Fuel-Sprayed Ni-Cr Coatings on 9Cr-1Mo Steel, *Metall. Mater. Trans. A*, 2004, **35**(10), p 3187-3199
6. T.S. Sidhu, S. Prakash, and R.D. Agrawal, Studies on the Properties of High-Velocity Oxy-Fuel Thermal Spray Coatings for Higher Temperature Applications, *Mater. Sci.*, 2005, **41**(6), p 805-823
7. E. Turunen, "Diagnostic Tools for HVOF Process Optimization," Ph.D. Thesis, Helsinki University of Technology, 2005
8. D. Cheng, Q. Xu, E.J. Lavernia, and G. Trapaga, The Effect of Particle Size and Morphology on the In-Flight Behavior of Particles During High-Velocity Oxy-Fuel Thermal Spraying, *Metall. Mater. Trans.*, 2001, **B32**(3), p 525-535
9. M.A. Uusitalo, P.M.J. Vuoristo, and T.A. Mäntylä, High Temperature Corrosion of Coatings and Boiler Steels in Reducing Chlorine-Containing Atmosphere, *Surf. Coat. Technol.*, 2002, **161**(2-3), p 275-285
10. T. Keller, W. Wagner, J. Ilavsky, J. Pisacka, G. Barbezat, and P. Fiala, Microstructure-Property Relationships and Cross-Property-Correlations of Thermal Sprayed Ni-Alloy Coatings, *Thermal Spray 2001: New Surfaces for a New Millennium*, C.C. Berndt, K.A. Khor, and E.F. Lugscheider, Ed., May 28-30, 2001 (Singapore), ASM International, 2001, p 643-652
11. J.R. Davis, Ed., *Handbook of Thermal Spray Technology*, Thermal Spray Society, ASM International, OH, 2004, p 338
12. F. Azarmi, T.W. Coyle, and J. Mostaghimi, Optimization of Atmospheric Plasma Spray Process Parameters using a Design of Experiment for Alloy 625 coatings, *J. Therm. Spray Tech.*, 2008, **17**(1), p 144-155
13. P. Fauchais, A. Vardelle, and B. Dussoubs, Quo Vadis Thermal Spraying?, *J. Therm. Spray Tech.*, 2001, **10**(1), p 44-66
14. H. Zhang, X.Y. Wang, L.L. Zheng, and X.Y. Jiang, Studies of Splat Morphology and Rapid Solidification During Thermal Spraying, *Int. J. Heat Mass Trans.*, 2001, **44**(24), p 4579-4592
15. J. Saaedi, T.W. Coyle, S. Mirdamadi, H. Arabi, and J. Mostaghimi, Phase Formation in a Ni-50Cr HVOF Coating, *Surf. Coat. Technol.*, 2008, **202**(24), p 5804-5811
16. R.K. Roy, Chapter 6, *A Primer on the Taguchi Method*, Society of Manufacturing Engineers (Dearborn, MI), 1990, p 100-125
17. V. Higuera, F.J. Belzunce, A. Carriles, and S. Poveda, Influence of the Thermal-Spray Procedure on the Properties of a Nickel-Chromium Coating, *J. Mater. Sci.*, 2002, **37**(3), p 649-654
18. E. Lugscheider, C. Herbst, and L. Zhao, Parameter studies on high-velocity oxy-fuel spraying of MCrAlY coatings, *Surf. Coat. Technol.*, 1998, **108-109**(1-3), p 16-23
19. A.D. Hewitt, Technology of Oxy-Fuel Gas Processes; Part 2: Comparative Combustion Properties of Fuel Gases, *Weld. Met. Fab.*, 1972, **40**, p 382-390
20. H.H. Tawfik and F. Zimmerman, Mathematical Modeling of the Gas and Powder Flow in HVOF Systems, *J. Therm. Spray Technol.*, 1997, **6**(3), p 345-352
21. M. Li and P.D. Christofides, Multi-Scale Modeling and Analysis of an Industrial HVOF Thermal Spray Process, *Chem. Eng. Sci.*, 2005, **60**, p 3649-3669

22. C.M. Hackett and G.S. Settles, Turbulent Mixing of the HVOF Thermal Spray and Coating Oxidation, *Thermal Spray Industrial Applications*, C.C. Bernt and S. Sampath, Ed., ASM Intentional, Boston, OH, USA, 1994, p 307-312
23. R.A. Neiser, M.F. Smith, and R.C. Dykhuizen, Oxidation in Wire HVOF-Sprayed Steel, *J. Therm. Spray Technol.*, 1998, **7**(4), p 537-545
24. K. Dobler, H. Kreye, and R. Schwetzke, Oxidation of Stainless Steel in the High Velocity Oxy-Fuel Process, *J. Therm. Spray Technol.*, 2000, **9**(3), p 407-413
25. K. Korpiola, ''High Temperature Oxidation of Metal, Alloy and Cermet Powders in HVOF Spraying Process,'' Ph.D. Thesis, Helsinki University of Technology, 2004, p 81
26. J. He, M. Ice, and E. Lavernia, Particle Melting Behavior During High-Velocity Oxygen Fuel Thermal Spraying, *J. Therm. Spray Technol.*, 2001, **10**(1), p 83-93
27. J.F. Li, H.L. Liao, C.X. Ding, and C. Coddet, Optimizing the Plasma Spray Process Parameters of Yttria Stabilized Zirconia Coatings Using a Uniform Design of Experiments, *J. Mater. Process. Technol.*, 2005, **160**(1), p 34-42